Research Square

Preprints are preliminary reports that have not undergone peer review.
They should not be considered conclusive, used to inform clinical practice,
or referenced by the media as validated information.

LncRNA BCYRN1 regulates mitochondrial MT-ND1/4/5 transcription via heavy strand promoter methylation to promote oxidative phosphorylation and proliferation in acute myeloid leukemia

Ye Kuang
Yan'an Hospital Affiliated To Kunming Medical University
Jia Wang
Yan'an Hospital Affiliated To Kunming Medical University
Jing Li
Yan'an Hospital Affiliated To Kunming Medical University
Chuanmei Peng
Yan'an Hospital Affiliated To Kunming Medical University
Yong Ji
Yan'an Hospital Affiliated To Kunming Medical University
Jinrong Tian
Yan'an Hospital Affiliated To Kunming Medical University
Sulian Chen
Yan'an Hospital Affiliated To Kunming Medical University
Shiyan Nian
Yan'an Hospital Affiliated To Kunming Medical University
Lei Feng
fenglei1@kmmu.edu.cn

Yan'an Hospital Affiliated To Kunming Medical University https://orcid.org/0000-0003-2731-1194

Research Article

Keywords: AML, MT-ND1/4/5, BCYRN1, IMT1B, OXPHOS, proliferation

Posted Date: July 7th, 2026

DOI: https://doi.org/10.21203/rs.3.rs-10158593/v1

License: This work is licensed under a Creative Commons Attribution 4.0 International License.
Read Full License

Abstract

Background

Acute myeloid leukemia (AML) is the most common adult acute leukemia. Treatment resistance and relapse remain the major clinical challenges. AML cells exhibit a unique dependence on mitochondrial oxidative phosphorylation (OXPHOS), which provides a promising metabolic vulnerability for targeted therapy.

Methods

Bioinformatic analysis was performed using integrated TCGA-LAML and GTEx public datasets. Bone marrow samples from 80 newly diagnosed AML patients and 80 normal controls were collected for clinical validation. Stable HL-60 cell lines with knockdown of BCYRN1 or mitochondrially encoded NADH dehydrogenase 1/4/5 (MT-ND1/4/5) were constructed. Cell biological behaviors and mitochondrial function were detected by CCK-8 assay, flow cytometry, Seahorse metabolic flux analysis, and transmission electron microscopy. The molecular regulatory mechanism was elucidated using RNA fluorescence in situ hybridization, subcellular fractionation, chromatin isolation by RNA purification, dual-luciferase reporter assay, and bisulfite sequencing PCR. A disseminated AML xenograft model was established to evaluate the in vivo anti-leukemic efficacy of both MT-ND1/4/5 knockdown and the mitochondrial RNA polymerase inhibitor IMT1B.

Results

AML cells displayed a predominant OXPHOS phenotype. MT-ND1, MT-ND4, and MT-ND5 were specifically upregulated and significantly associated with poor prognosis in AML patients. Knockdown of MT-ND1/4/5 significantly inhibited AML cell proliferation, induced apoptosis, disrupted mitochondrial structural integrity, and reduced OXPHOS activity in vitro. In vivo experiments further confirmed that MT-ND1/4/5 knockdown markedly suppressed leukemic cell dissemination in xenograft mice. lncRNA BCYRN1 was significantly upregulated in AML and associated with poor prognosis. BCYRN1 is present in the mitochondrial compartment. It transcriptionally activates MT-ND1/4/5 through two coupled actions: direct binding to mitochondrial heavy-strand promoter 1, and subsequent promotion of methylation at the m.545C site. Knockdown of BCYRN1 recapitulated the phenotypes of MT-ND1/4/5 knockdown, suppressing OXPHOS and proliferation of AML cells. Finally, the RNA polymerase mitochondrial (POLRMT) inhibitor IMT1B repressed mitochondrial transcription, significantly downregulated MT-ND1/4/5 expression, and effectively inhibited AML progression both in vitro and in vivo.

Conclusion

We demonstrate that mitochondria-localized lncRNA BCYRN1 epigenetically activates mitochondrial transcription to promote OXPHOS and AML progression. Targeting either genetically (MT-ND1/4/5 knockdown) or pharmacologically (IMT1B) effectively inhibits proliferation of AML cells, establishing it as a novel prognostic biomarker and therapeutic target for AML.

Introduction

Acute myeloid leukemia (AML), the most common adult acute leukemia, is a genetically heterogeneous hematologic malignancy driven by clonal differentiation-arrested myeloid progenitors, which impairs hematopoiesis and causes fatal complications [1, 2]. With a median diagnostic age of 68 years, it has 5-year overall survival ~ 24% [3]. The "7 + 3" induction chemotherapy is the standard first-line intensive regimen for fit AML patients, followed by post-remission consolidation therapy or allo-HSCT. Targeted and immunotherapeutic approaches are available for patients ineligible for intensive chemotherapy [4, 5]. Despite these advances in AML therapy, primary treatment failure and high relapse rates stem largely from chemoresistant leukemia stem cells (LSCs) and inherent disease heterogeneity, and remain the most pressing clinical challenges to address [6, 7].

Metabolic heterogeneity and reprogramming are defining features of AML that promote malignant cell survival, proliferation and treatment resistance. Notably, reliance on mitochondrial oxidative phosphorylation (OXPHOS) represents a dominant, druggable metabolic phenotype in this disease [8, 9]. Unlike the Warburg effect (aerobic glycolysis dominance) in most solid tumors, AML cells are uniquely addicted to OXPHOS rather than glycolysis for ATP production [10]. LSCs possess a limited ability to upregulate glycolysis as a compensatory mechanism when mitochondrial respiration is inhibited. This metabolic constraint renders OXPHOS a unique and specific vulnerability that can be exploited to eradicate the relapse-driving leukemic clones [11]. Clinically, elevated OXPHOS activity is tightly associated with adverse outcomes, treatment resistance, and disease relapse in AML [12]. Thus, targeting OXPHOS holds great promise to overcome therapeutic resistance and improve clinical outcomes for AML patients [13–15].

Brain cytoplasmic RNA 1 (BCYRN1), a well-characterized neuronal-derived long non-coding RNA, acts as a pivotal oncogenic regulator in multiple human malignancies. Its aberrant expression drives malignant cell proliferation, invasion, stemness maintenance and therapeutic resistance via diverse signaling pathways in solid tumors (lung, hepatocellular and prostate cancer) [16–18]. However, the expression, functions and mechanisms of BCYRN1 in AML remain largely uncharacterized, especially its role in mitochondrial OXPHOS reprogramming that drives AML cell survival.

Using multiple AML models, we show BCYRN1 is upregulated in clinical AML samples. It enhances the mitochondrial heavy strand promoter 1 (HSP1) methylation to promote mtDNA transcription and MT-ND1/4/5 expression, thus augmenting OXPHOS. Both BCYRN1/MT-ND1/4/5 silencing and IMT1B-mediated mitochondrial transcription inhibition markedly suppress OXPHOS, inhibit proliferation and trigger apoptosis in AML cells. Taken together, our study identifies BCYRN1 as a novel regulator of

OXPHOS in AML via modulating mtDNA transcription, providing a promising prognostic biomarker and therapeutic target for AML. Consistently, mtDNA transcription inhibitors hold promise as a novel therapeutic approach for AML.

Materials and Methods

Primary patient specimens

A total of 80 cases of bone marrow aspirate supernatant from AML patients (M0-M7 subtypes) and 80 cases from normal individuals were collected and centrifugally separated from the Affiliated Yan'an Hospital of Kunming Medical University between 2024 and 2025. The diagnostic criteria for all AML patients were based on the French-American-British (FAB) classification and National Comprehensive Cancer Network (NCCN) guidelines. We excluded patients with prior anti-leukemic therapy before bone marrow sampling, concomitant active malignancies, severe systemic comorbidities (severe hepatorenal dysfunction, uncontrolled severe infection, active autoimmune disease) that could bias molecular and metabolic assay results, pregnancy, or lactation. The study protocol was approved by the Ethics Committee of Yan'an Hospital affiliated to Kunming Medical University (Approval number: 2024-013-01). All participants provided written informed consent before enrollment.

Cell culture

In this study, a total of 8 human AML cell lines representing all FAB classification subtypes (M0 to M7), namely MOLM-16 (M0, Cat. CBP60241), KG-1a (M1, Cat. CBP61455), HL-60 (M2, Cat. CBP60517), NB4 (M3, Cat. CBP61443), OCI-AML2 (M4, Cat. CBP60527), MOLM-13 (M5, Cat. CBP60678), TF1 (M6, Cat. CBP60808) and MEG-01 (M7, Cat. CBP61104), were used as in vitro models, with all cell lines purchased from Nanjing Kebai Biotechnology Co., Ltd. The culture media (RPMI 1640, Cat. 11875101, Thermo Fisher Scientific Inc.) were supplemented with 10% (v/v) fetal bovine serum (FBS, Cat. A5669701, Thermo Fisher Scientific Inc.) and 1% (v/v) penicillin-streptomycin solution (Cat. 15140148, Thermo Fisher Scientific Inc.), with cells incubated at 37°C in a humidified atmosphere containing 5% CO_2.

Cell transfection

Stable BCYRN1 knockdown and MT-ND1/4/5 triple-knockdown HL-60 cell lines were established using a mitochondrially targeted dLwaCas13a-mBN-MLS lentiviral system. The pLKO.1-based vector harbors a dual-expression cassette: the PGK promoter drives the MLS-dLwaCas13a-mBN fusion protein for targeted mitochondrial RNA degradation, and the U6 promoter drives gRNA transcription with a 5' mitochondrial import motif. Two independent gRNAs were designed for BCYRN1 to reduce off-target risk, while a tandem tRNA-gRNA array was constructed for synchronous expression of three MT-ND1/4/5-targeting gRNAs. For the overexpression vector, the full-length BCYRN1 sequence fused with a 5'5S rRNA mitochondrial import motif was driven by the PGK promoter to direct the transcripts into the

mitochondrial matrix via the endogenous RNA transport pathway. Lentiviruses were packaged in HEK293T cells with the second-generation system (psPAX2/pMD2.G). HL-60 cells were transduced via spin infection (MOI 10–30, polybrene), selected with puromycin for 7 days, and monoclonally isolated by limiting dilution. Positive clones were verified for knockdown efficiency by Western blot and RT-qPCR.

AML animal model

A total of 25 female NCG mice (6–8 weeks old, Strain: T001475, GemPharmatech Inc.) were randomly divided into 5 groups (n = 5): (1) normal control; (2) HL-60-luc-NC; (3) HL-60-luc-MT-ND1/4/5 KD; (4) HL-60-luc + vehicle; (5) HL-60-luc + IMT1B. Mice were housed under SPF conditions with 12 h light/dark cycle. In vivo bioluminescence imaging (BLI) was performed on days 7, 14 and 20 for groups 1–3 to monitor leukemia burden, and on days 0, 15 and 30 for groups 1, 4 and 5 to evaluate the therapeutic effect. At endpoints, bone marrow cells were stained with anti-mCD45, hCD45, hCD13, hCD33 and hCD117 antibodies, and the percentage of corresponding CD-positive AML cells was analyzed by flow cytometry. Peripheral blood was collected for complete blood count. Spleens were harvested, weighed and photographed. Bone marrow smears were stained with Wright-Giemsa. Humane endpoints included > 15% body weight loss, severe debilitation, dyspnea or paralysis. Mice reaching any humane endpoint were immediately euthanized by CO_2 asphyxiation. This study was approved by the Institutional Animal Care and Use Committee of Yan'an Hospital Affiliated to Kunming Medical University (Approval number: 2023021) and conducted in accordance with ARRIVE guidelines.

Reverse Transcription Quantitative PCR (RT-qPCR)

Intact mitochondria were first isolated using a differential centrifugation-based mitochondrial isolation kit (Cat. C3601, Beyotime Biotechnology Co., Ltd.) from the cells and primary bone marrow mononuclear cells (BMMCs) according to the manufacturer's instructions. Mitochondrial RNA (mtRNA) was extracted from the cells using TRIzol reagent (Cat. AM9738, Thermo Fisher Scientific Inc.) following the manufacturer’s instructions, and reverse-transcribed into complementary DNA (cDNA) with the PrimeScript RT Reagent Kit (Cat. RR037Q, Takara Biomedical Technology Co., Ltd). QPCR was performed on the Real-Time PCR System (Model:7500, Thermo Fisher Scientific Inc.) using SYBR Premix Ex Taq Kit (Cat. DRR041A, Takara Biomedical Technology Co., Ltd.). Mitochondrial 16S rRNA served as the reference. The relative expression levels of target genes were calculated via the 2^-ΔΔCt method, with all experiments performed in three independent biological replicates. The following primer sequences were used: MT-ND1 forward, 5'-CATTGTTCGCATAGCCGATA-3' and reverse, 5'-CGCGATGTTCATTACCAGTTT-3'; MT-ND4 forward, 5'-CTTCGAAACCACACTTATCC-3' and reverse, 5'-GTATGCAATGAGCGATTTTAGG-3'; MT-ND5 forward, 5'-CACTGAGTCACCATAAATTCAATAGAACT-3' and reverse, 5'-TGTGACAAAAAGGGCTACAGATGT-3'; BCYRN1 forward, 5'-ATAGCTTGAGCCCAGGAGTT-3'; BCYRN1 reverse, 5'-ATAAGACCGTAGCACACATCTAA-3'; mitochondrial 16S rRNA, Forward, 5'-CACTGCCTGCCCAGTGA-3' and reverse: 5'-ATACCGCGGCCGTTAAA-3'.

Western blot

The purified mitochondrial pellets were lysed in RIPA lysis buffer (Cat. P0038, Beyotime Biotechnology Co., Ltd.) supplemented with 1% phenylmethanesulfonyl fluoride (PMSF) to obtain mitochondrial protein fractions. Protein concentration was quantified using the Bicinchoninic Acid (BCA) Protein Assay Kit (Cat. P0010, Beyotime Biotechnology Co., Ltd.). Equal amounts of protein samples (20–30 μg per lane) were separated by 10% sodium dodecyl sulfate-polyacrylamide gel electrophoresis (SDS-PAGE), and then electrotransferred onto polyvinylidene fluoride (PVDF) membranes (Cat. IPFL00010, Merck KGaA). After blocking with 5% non-fat milk dissolved in Tris-buffered saline containing 0.1% Tween-20 (TBST, Cat. ST671, Beyotime Biotechnology Co., Ltd.) for 1 h at room temperature, the membranes were incubated overnight at 4°C with primary antibodies against MT-ND1 (Cat. ab181848, 1:3000), MT-ND4 (Cat. A17970, ABclonal, Inc., 1:1000), MT-ND5 (Cat. ab230509, Abcam Inc., 1:3000) and VDAC1 (Cat. A19707, ABclonal, Inc., 1:5000) from Abcam plc. Subsequently, the membranes were washed 3 times with TBST (10 min each), and incubated with corresponding horseradish peroxidase (HRP)-conjugated secondary antibodies (1:10000, Cat. ab6721, Abcam plc) for 1 h at room temperature. After repeated TBST washes, protein bands were visualized using an enhanced chemiluminescence (ECL) detection kit (Cat. 34579, Thermo Fisher Scientific Inc.) on a maging system (Model: ChemiDoc XRS+, Bio-Rad Laboratories Inc.). Grayscale values of target bands were quantified via Image J software (Version 1.54p, National Institutes of Health).

Seahorse XF metabolic flux assay

Mitochondrial respiration and glycolysis were assessed by detecting oxygen consumption rate (OCR) and extracellular acidification rate (ECAR) respectively with seahorse analyzer (model: XF96, Agilent Technologies, Inc.). For OCR detection, cells were equilibrated in supplemented XF base medium, and OCR was measured under basal conditions and after serial injection of oligomycin (1 μM), carbonyl cyanide 4-(trifluoromethoxy) phenylhydrazone (FCCP, 1.5 μM), and rotenone & antimycin A (0.5 μM each). For ECAR detection, cells were equilibrated in glucose-free XF base medium, and ECAR was recorded sequentially after injection of D-glucose (10 mM), oligomycin (1 μM), and 2-deoxy-D-glucose (2-DG, 50 mM). Key respiratory and glycolytic parameters were calculated respectively.

Mitochondrial respiratory chain complex activity assay

The enzymatic activities of mitochondrial respiratory chain complexes I–V were measured using colorimetric microplate kits (Nanjing Jiancheng Bioengineering Institute) following the manufacturer's instructions. The catalog numbers are as follows: complex I (Cat. A089-1-1), complex II (Cat. A089-2-1), complex III (Cat. A089-3-1), complex IV (Cat. A089-4-1), and complex V (Cat. A089-5-1). Absorbance was detected on a microplate reader, and relative enzyme activities were calculated against the control group.

Mitochondrial function and ultrastructure assay

Mitochondrial superoxide production, mitochondrial membrane potential, and mitochondrial ultrastructure were assessed using MitoSOX Red (Cat. M36007, Thermo Fisher Scientific Inc.) staining, JC-1 (Cat. M34152, Thermo Fisher Scientific Inc.) staining, and transmission electron microscopy (TEM, Model: JEM-1400, JEOL Ltd.), respectively. Briefly, cells were incubated with 5 μM MitoSOX Red for 30 min at 37°C in the dark, and mitochondrial superoxide levels were quantified via flow cytometry. In parallel, cells were stained with 10 μM JC-1 probe for 20 min at 37°C under light-protected conditions, and the ratio of JC-1 aggregate to monomer fluorescence was detected by flow cytometry to evaluate mitochondrial depolarization. To visualize mitochondrial ultrastructure including cristae integrity and morphological changes, cells were fixed, dehydrated, embedded, sectioned and double-stained, followed by observation and imaging via a TEM.

RNA fluorescence In situ hybridization (FISH) for mitochondrial co-localization

Mitochondrial localization of BCYRN1, MT-ND1, MT-ND4 and MT-ND5 was verified by single-molecule RNA FISH (smFISH) with mitochondrial and nuclear co-staining. Briefly, HL-60 cells were pre-labeled with MitoTracker Green (Cat. C1048, Beyotime Biotechnology Co., Ltd.) to mark mitochondria and hybridized overnight at 37°C with a pool of 3'-fluorescently labeled target-specific smFISH probes against BCYRN1, MT-ND1, MT-ND4 and MT-ND5. The sequences of all smFISH probes were shown in Supplementary Table S1. Nuclei were counterstained with DAPI for 5 min. Fluorescence images were acquired with a KF-FL-020 digital pathological slide scanner (KONFOONG BIOINFORMATION TECH CO., LTD.).

Cell viability and apoptosis assays

Cell viability of cells subjected to different treatments was evaluated by cell counting kit-8 (CCK-8) assay (Cat. C0037, Beyotime Biotechnology Co., Ltd.), with absorbance detected at 450 nm using a microplate reader (Model: A51119700DPC, Thermo Fisher Scientific Inc.). Cell apoptosis was quantified by Annexin V/PI double staining (Cat. C1383S, Beyotime Biotechnology Co., Ltd.), followed by flow cytometry. Total apoptotic rate was defined as the sum of early and late apoptotic cell populations.

Chromatin isolation by RNA purification assay

HL-60 cells were crosslinked with 1% formaldehyde, lysed, and sonicated to generate 100–500 bp chromatin fragments. Equal aliquots of lysate were incubated with 3' biotin-labeled LacZ non-specific control probe set, BCYRN1 odd non-overlapping probe set, and BCYRN1 even non-overlapping probe set, respectively. Equal lysate aliquots were incubated with 3'-biotin-labeled LacZ control probe set (10 probes) and non-overlapping BCYRN1 probe sets (4 probes), respectively. Probe sequences are in Supplementary Table S3. Probe-bound RNA-DNA complexes were captured by streptavidin magnetic beads, washed, then crosslinks reversed, DNA eluted and purified. Target regions (GAPDH nuclear control, HSP1-1/1–2, HSP2-1/2–2) in CHIRP and Input samples were quantified by qPCR, with enrichment calculated as CHIRP/Input ratio. The primers for HSP1-1, HSP1-2, HSP2-1, and HSP2-2 are as

follows: HSP1-1 forward, 5'-TCCCACTCCCATACTACTAATC-3' and reverse, 5'-ATAAACTGTGGGGGGTGTCT-3'; HSP1-2 forward, 5'-TCCCACTCCCATACTACTAATCTCAT-3' and reverse, 5'-ATAAACTGTGGGGGGTGTCTTTG-3'; HSP2-1 forward, 5'-TTAGACGGGCTCACATCACC-3' and reverse, 5'-CTGCGTGCTTGATGCTTGTT-3'; HSP2-2 forward, 5'-ATCCCCGTTCCAGTGAGTTC-3' and reverse, 5'-GCTAGGCTAAGCGTTTTGAGC-3'.

Dual luciferase reporter gene assay

The wild-type HSP1 promoter and its mutant derivative (with the predicted core BCYRN1 binding region mutated to consecutive AAA residues) were cloned into the promoterless pGL3-Basic vector (Cat. 212936, Addgene Inc.). To reconstitute the mitochondrial transcription machinery in the nucleus, plasmids expressing nuclear-localized human POLRMT, TFAM and TFB2M were co-delivered in all groups. All three constructs were based on the pcDNA3.1(+) backbone (Cat. 208051, Addgene Inc.), lacked the N-terminal mitochondrial targeting sequence, and contained a C-terminal SV40 nuclear localization signal to ensure nuclear retention. Full-length human BCYRN1 was cloned into the pcDNA3.1(+) mammalian expression vector, with empty pcDNA3.1(+) used as the negative control. The pRL-TK vector (Cat. 1324, Addgene Inc.) was co-transfected in all groups as an internal control for transfection efficiency. HEK293T cells were transfected using Lipofectamine 3000 and HL-60 cells were transfected by electroporation. Luciferase activities were measured 48 h post-transfection with the Dual-Luciferase Reporter Assay System (Cat. E1910, Promega Biotech Co., Ltd). The relative promoter activity was presented as the firefly/Renilla luciferase ratio.

BCYRN1 mediates HSP1 methylation

Total cellular DNA was isolated from empty vector control and BCYRN1-overexpressing AML cells. Sodium bisulfite conversion was performed using the EZ DNA Methylation-Gold Kit (Cat. D5006, Zymo Research Corporation) according to the manufacturer's instructions, with conversion efficiency verified using a fully unmethylated control DNA. PCR products were cloned into the pJET1.2 blunt-end vector (Cat. K1231, Thermo Fisher Scientific Inc.). At least 20 positive clones per sample were Sanger sequenced to ensure adequate statistical power for detecting low-level methylation changes in mitochondrial DNA. Methylation levels at the m.545C site were quantified using BiQ Analyzer software 3.0 software.

Statistical analysis

All analyses were performed using R software (version 4.3.1) and Statistical Product and Service Solutions (SPSS, version: 29.0). Transcriptomic data of AML patients from The Cancer Genome Atlas (TCGA) and normal peripheral blood samples from the Genotype-Tissue Expression (GTEx) database were integrated, batch-corrected using ComBat-seq, and transformed to $\log_2(\text{TPM} + 1)$. Differential expression of mitochondrial genes MT-ND1/2/3/4/4L/5/6 and lncRNA BCYRN1 was analyzed using limma-voom pipeline ($|\log_2(\text{fold change})| > 1$, FDR < 0.05). For survival analysis, TCGA-LAML patients and our in-house cohort of 80 AML patients were stratified by median gene expression, with Kaplan-Meier curves and log-rank tests generated. Pearson correlation coefficient was used to explore associations

between BCYRN1 and MT-ND1/4/5 in AML groups. The data were presented as mean ± SD of at least 3 biological replicates. Student's t-test was used for comparisons between two groups, and one-way ANOVA with Tukey's post-hoc test for comparisons among three or more groups. All tests were two-sided, with $p < 0.05$ considered significant.

Results

Elevated mitochondrial complex I mediates a dominant OXPHOS energetic advantage in AML cells

The Seahorse XF analysis showed that AML BMMCs exhibited significantly elevated overall OCR curves compared with normal controls. Consistently, the key mitochondrial respiration parameters, including basal OCR, ATP-linked OCR, maximal OCR and spare respiratory capacity, were all significantly higher in AML patients than in normal controls ($P < 0.05$, Fig. 1A, B). In contrast, the overall ECAR curves of AML BMMCs were significantly lower than those of normal controls. Correspondingly, the core glycolytic indicators, including basal glycolysis, glycolytic capacity, and glycolytic reserve, were all substantially reduced in AML patients relative to normal controls ($P < 0.05$, Fig. 1C, D).

ELISA analysis the activity of mitochondrial complex I-V revealed that only complex I was significantly increased (3.21 ± 0.28-fold, $P < 0.001$) in AML BMMCs, while complexes II-V showed no significant difference between AML and normal controls (Fig. 1E). CCK-8 assays performed on a panel of 8 AML cell lines covering M0-M7 subtypes demonstrated that both hypoxia (1% O_2) and treatment with 0.5 μM of each mitochondrial complex I inhibitors (rotenone or AR-054) significantly reduced cell viability in all tested cell lines ($P < 0.05$, Fig. 1F-H), indicating a broad dependence on complex I activity in AML.

MT-ND1/4/5 overexpression and their prognostic significance in AML

We first performed differential expression analysis using the TCGA-LAML and GTEx healthy whole blood datasets. The results showed that mRNA levels of MT-ND1, MT-ND4 and MT-ND5 were significantly upregulated in AML samples, while no significant differences were found in the mRNA levels of other subunits (MT-ND2, MT-ND3, MT-ND4L, MT-ND6) between AML and normal controls (Fig. 2A). We further validated these findings in an independent cohort of 80 de novo AML patients and 80 normal controls. RT-qPCR and western blot consistently confirmed that the mRNA and protein levels of MT-ND1/4/5 were significantly elevated in BMMC specimens from AML patients, with no significant changes in other subunits, which was fully consistent with our bioinformatics results (Fig. 2B, C). Survival analysis using both the TCGA-LAML cohort and our in-house clinical cohort revealed that high expression of MT-ND1, MT-ND4 and MT-ND5 was significantly associated with inferior overall survival (OS) in AML patients (Fig. 2D, E), suggesting these subunits as potential adverse prognostic biomarkers for AML.

MT-ND1/4/5 KD inhibits AML cell survival in vitro and in vivo

To verify the functional role of MT-ND1, MT-ND4 and MT-ND5 in AML cells, we established stable HL-60 cell lines with both single and combined knockdown of MT-ND1/4/5. RT-qPCR confirmed significant downregulation of the corresponding target mRNA in single-gene silencing cells ($P < 0.001$, Fig. 3A), and both RT-qPCR and western blot verified markedly reduced mRNA and protein levels of all three subunits in the MT-ND1/4/5 co-silencing group, compared with the NC group ($P < 0.001$, Fig. 3B). CCK-8 assay showed that either single or combined silencing of MT-ND1/4/5 significantly inhibited HL-60 cell viability ($P < 0.001$, Fig. 3C). Consistently, Annexin V-PI flow cytometric analysis revealed a significant increase in apoptotic cell proportion in all silencing groups ($P < 0.001$, Fig. 3D), indicating that MT-ND1, MT-ND4 and MT-ND5 are essential for AML cell survival.

To validate the in vivo role of MT-ND1/4/5 in AML, we established a disseminated xenograft model by tail vein injection of PBS, HL-60-NC or HL-60-MT-ND1/4/5 KD cells into NCG mice, with a 20-day observation period for AML engraftment (Fig. 3E). As shown in Fig. 3F, in vivo bioluminescence imaging showed that the HL-60-NC and HL-60-MT-ND1/4/5 KD groups had more bioluminescent foci and higher mean radiance than the PBS group ($P < 0.001$), while these indicators were significantly reduced in the HL-60-MT-ND1/4/5 KD group compared with the HL-60-NC group ($P < 0.001$). Flow cytometric analysis revealed that the HL-60-NC group had a lower proportion of mCD45 + cells and higher proportions of hCD45+, hCD13+, hCD33 + and hCD34 + cells versus the PBS group ($P < 0.001$). In contrast, MT-ND1/4/5 KD reversed these changes, with increased mCD45 + proportion and decreased infiltration of human AML cells in the bone marrow ($P < 0.001$, Fig. 3G).

MT-ND1/4/5 KD impairs mitochondrial energy metabolism in AML cells

The results showed that the catalytic activity of mitochondrial complex I, ATP production and the NAD^+/NADH ratio were significantly reduced in mitochondria isolated from HL-60-MT-ND1/4/5 KD cells and BMMCs from MT-ND1/4/5 KD xenografts ($P < 0.05$, Fig. 4A-C). Seahorse analysis revealed that MT-ND1/4/5 KD significantly impaired mitochondrial OXPHOS, with basal OCR, ATP-linked OCR, maximal OCR and spare respiratory capacity all decreased compared with NC cells ($P < 0.001$, Fig. 4D). In response to OXPHOS dysfunction, MT-ND1/4/5 KD cells exhibited compensatory glycolytic reprogramming, with significantly increased basal glycolysis ($P < 0.05$), glycolytic reserve ($P < 0.05$) and glycolytic capacity ($P < 0.001$, Fig. 4E). Mitochondrial membrane potential was detected by JC-1 staining. Flow cytometric analysis showed that the proportion of JC-1 monomers was significantly increased, while the proportion of JC-1 aggregates was decreased in HL-60-MT-ND1/4/5 KD cells ($P < 0.001$, Fig. 4F). MitoSOX Red staining revealing elevated mitochondrial superoxide levels in MT-ND1/4/5 KD cells compared with negative controls (Fig. 4E, F). Finally, TEM was used to observe mitochondrial ultrastructure. Compared with NC cells, HL-60-MT-ND1/4/5 KD cells showed a significant reduction in

mitochondrial number per cell ($P < 0.001$), a marked increase in the proportion of abnormal mitochondria ($P < 0.001$), and a decreased number of mitochondrial cristae per mitochondrion ($P < 0.01$, Fig. 4H).

lncRNA BCYRN1 regulates MT-ND1/4/5 by interaction with HSP1

Correlation analysis using the TCGA-LAML dataset revealed that BCYRN1 expression was significantly positively correlated with the mRNA levels of MT-ND1, MT-ND4 and MT-ND5 in AML patients (all $P < 0.001$, Fig. 5A). The joint analysis results of the TCGA and GTEx databases indicated that BCYRN1 expression was significantly elevated in AML samples compared with normal controls ($\log_2FC = 4.5$, $P < 0.001$, Fig. 5B). Survival analysis demonstrated that patients with high BCYRN1 expression had significantly shorter overall survival than those with low BCYRN1 expression ($P < 0.001$, Fig. 5C). Further validation in our clinical cohort showed that BCYRN1 was significantly upregulated in BMMCs from AML patients compared with normal controls ($P < 0.001$, Fig. 5D). To determine whether BCYRN1 regulates the expression of MT-ND1/4/5, we established stable BCYRN1-knockdown (BCYRN1 KD) HL-60 cell line ($P < 0.001$, Fig. 5E). Notably, the mRNA levels of MT-ND1, MT-ND4 and MT-ND5 were all significantly downregulated in BCYRN1 KD cells ($P < 0.001$, Fig. 5F), which was further verified at the protein level by western blot analysis (Fig. 5G). Subcellular localization analysis using FISH combined with MitoTracker staining revealed that BCYRN1 was predominantly localized in the mitochondria of HL-60 cells and colocalized with MT-ND1, MT-ND4 and MT-ND5 (Fig. 5H). Subcellular fractionation followed by qPCR further confirmed that BCYRN1 was highly enriched in the mitochondrial fraction, with minimal expression in the cytoplasmic and nuclear fractions ($P < 0.001$ vs whole cell, Fig. 5I). To investigate the molecular mechanism by which BCYRN1 regulates MT-ND1/4/5 expression, we performed chromatin isolation by RNA purification (CHIRP) assay to identify genomic regions bound by BCYRN1. The results showed that both odd-numbered and even-numbered BCYRN1 probe sets specifically bound to HSP1, but not to HSP2 ($P < 0.001$, Fig. 5J). Dual-luciferase reporter assay was performed to verify the molecular interaction between BCYRN1 and HSP1. Co-transfection of full-length BCYRN1 and HSP1 markedly increased luciferase activity ($P < 0.001$). Mutation of the HSP1 binding site 1 alone did not obviously alter the luciferase signal. In contrast, mutation of binding site 2 or site 3 significantly reduced luciferase activity. Consistent results were further validated in HEK293T cells, confirming that BCYRN1 interacts with HSP1 mainly through binding sites 2 and 3 rather than site 1 (Fig. 5K, L). Finally, BSP analysis showed that overexpressed BCYRN1($P < 0.001$, Fig. 5M) significantly increased the methylation level of the functional m.545C site within the HSP1 in both HL-60 and HEK293T cells ($P < 0.001$, Fig. 5N).

lncRNA BCYRN1 regulates energy metabolism and cell survival in AML

CCK-8 assay showed that BCYRN1 KD significantly inhibited HL-60 cell viability by 26.71 ± 3.81% of the NC group ($P < 0.001$, Fig. 6A). Intracellular ATP production was also markedly decreased in BCYRN1 KD cells ($P < 0.001$, Fig. 6B). Annexin V-PI flow cytometric analysis further revealed that BCYRN1 KD induced

a significant increase in the proportion of apoptotic cells ($P < 0.001$, Fig. 6C), indicating that BCYRN1 is essential for AML cell survival. We next investigated the impact of BCYRN1 KD on mitochondrial function. JC-1 staining demonstrated that BCYRN1 knockdown resulted a significant increase in the proportion of JC-1 monomers-positive cells and a corresponding decrease in JC-1 aggregates-positive cells ($P < 0.001$, Fig. 6D). MitoSOX Red staining showed that mitochondrial superoxide levels were markedly elevated in BCYRN1 KD cells compared with NC cells ($P < 0.001$, Fig. 6E, F). TEM was used to observe mitochondrial ultrastructural changes. Quantitative analysis revealed that BCYRN1 KD significantly reduced the number of mitochondria per cell, increased the proportion of abnormal mitochondria, and decreased the number of mitochondrial cristae per mitochondrion ($P < 0.05$, Fig. 6E, F). Finally, the OCR curve showed that BCYRN1 KD significantly impaired mitochondrial respiratory function in HL-60 cells. Quantitative analysis demonstrated that basal OCR, ATP-linked OCR, maximal OCR, and spare respiratory capacity were all markedly reduced in the BCYRN1 KD group compared with the NC group ($P < 0.001$, Fig. 6H).

Therapeutic efficacy of IMT1B in a disseminated AML xenograft model

We evaluated the therapeutic potential of IMT1B (Synonyms: LDC203974), a POLRMT inhibitor. In vitro, 1 μM IMT1B significantly downregulated the mRNA and protein levels of MT-ND1/4/5 (all $P < 0.001$, Fig. 7A,B) and reduced the activity of complex I in HL-60 cells ($P < 0.001$, Fig. 7C). Consistently, IMT1B markedly impaired OXPHOS, with significant reductions in basal, ATP-linked, maximal OCR and spare respiratory capacity ($P < 0.001$, Fig. 7D). IMT1B treatment also decreased HL-60 cell viability and intracellular ATP levels to 16.87 ± 2.90% and 26.60 ± 2.33% of the control group, respectively ($P < 0.001$, Fig. 7E, F).

To evaluate the in vivo anti-leukemic efficacy of IMT1B, we established a disseminated HL-60-luc AML xenograft model in NCG mice. Mice were randomized to receive daily oral administration of vehicle or IMT1B (10 mg/kg) starting on day 15 post-inoculation (Fig. 7G). Bioluminescence imaging demonstrated that IMT1B treatment significantly inhibited tumor progression, with markedly reduced bioluminescence intensity at day 30 ($P < 0.001$, Fig. 7H). IMT1B treatment could attenuated body weight loss in AML mice ($P < 0.001$, Fig. 7I). IMT1B treatment also decreased white blood cell counts while increasing red blood cell and platelet counts (all $P < 0.001$, Fig. 7J). Wright-Giemsa staining of bone marrow. Normal controls show intact hematopoietic architecture with complete granulocytic differentiation; AML mice exhibit massive leukemic blast infiltration (> 20%), high nuclear-cytoplasmic ratio, extensive cytoplasmic vacuoles and reduced mature myeloid cells. IMT1B treatment partially reversed the above phenotypes, as evidenced by reduced leukemic blast infiltration, diminished cytoplasmic vacuoles and partial recovery of normal myeloid differentiation (Fig. 7K). Furthermore, IMT1B significantly reduced spleen weight ($P < 0.001$, Fig. 7L). Flow cytometric analysis revealed decreased hCD45 + leukemic cells and increased proportions of mature myeloid cells (hCD13+, hCD33+) and hematopoietic stem/progenitor cells (hCD117+) in bone marrow (all $P < 0.001$, Fig. 7M).

Discussion

AML is a highly heterogeneous hematological malignancy characterized by the clonal expansion of immature myeloid blasts in the bone marrow [19]. The majority of patients eventually develop drug resistance and relapse, and the prognosis for relapsed/refractory AML is particularly poor, with a 3-year overall survival rate of less than 24% even after allogeneic hematopoietic cell transplantation [20]. The lack of effective targeted therapies for this high-risk patient population highlights the urgent need to identify novel molecular mechanisms and therapeutic vulnerabilities in AML.

In this study, we systematically investigated the role and mechanism of lncRNA BCYRN1 in AML progression. We first demonstrated that BCYRN1 is significantly upregulated in AML patient samples and associated with poor prognosis. Mechanistically, BCYRN1 localizes to mitochondria and activates HSP1-driven transcription of MT-ND1/4/5 by modulating m.545C site methylation of the HSP1 promoter. This leads to enhanced mitochondrial complex I activity and OXPHOS, which is essential for AML cell survival and energy metabolism. Finally, we provided preclinical evidence that IMT1B, a selective mitochondrial RNA polymerase inhibitor, exerts potent anti-leukemic activity both in vitro and in vivo, and alleviates AML-induced hematopoietic suppression.

Unlike most solid tumors that rely on aerobic glycolysis (the Warburg effect) for energy production, AML cells exhibit a unique metabolic phenotype characterized by a predominant dependence on OXPHOS [21]. This metabolic vulnerability was identified by Lagadinou et al. in 2013, who proposed a model wherein the unique physiology of ROS-low LSCs provides an opportunity for selective targeting via disruption of BCL-2-dependent OXPHOS [22]. Subsequent studies have confirmed that not only LSCs but also bulk AML cells and minimal residual disease (MRD) cells after chemotherapy are highly addicted to OXPHOS [23–25]. This metabolic phenotype makes mitochondrial OXPHOS an attractive therapeutic target for AML [26, 27]. However, the upstream regulatory mechanisms governing OXPHOS in AML remain largely unknown, limiting the development of effective targeted therapies.

Mitochondrial complex I serves as the initial and rate-limiting complex of the mitochondrial electron transport chain. Its three core hydrophobic subunits are encoded by the mitochondrial genes MT-ND1, MT-ND4 and MT-ND5 respectively [28]. While mutations in these genes have been reported in various cancers, including colorectal cancer [29], renal cell carcinoma [30] and gastric cancer [31], their dysregulation and functional contribution to AML pathogenesis remain poorly understood. lncRNA BCYRN1, also known as BC200, has previously been implicated in the progression of several solid tumors. BCYRN1 functions as an oncogene by regulating various cellular processes, such as sponging microRNAs [32], regulating gene expression [33] and promoting epithelial-mesenchymal transition [34]. Our study is the first to demonstrate that BCYRN1 can localize in mitochondria that directly regulates mtDNA gene expression through epigenetic modification of the HSP1. This finding not only expands our understanding of the biological functions of BCYRN1 but also reveals a novel mechanism of mitochondrial gene regulation.

Given the critical role of complex I activation in AML progression, we further explored the therapeutic potential using IMT1B [35], a specific POLRMT inhibitor. Several mitochondrial complex I inhibitors have been developed for cancer treatment, including IACS-010759, which showed promising preclinical activity in AML models [36]. However, phase I clinical trials of IACS-010759 were discontinued due to a narrow therapeutic index, with dose-limiting toxicities including elevated blood lactate and neurotoxicity [37]. IMT1B (LDC203974) is a first-in-class, orally bioavailable allosteric inhibitor of POLRMT. It binds to a unique POLRMT allosteric pocket to block mitochondrial DNA transcription and OXPHOS, exhibiting a wider therapeutic index and minimal normal tissue toxicity compared with conventional complex I inhibitors due to the greater metabolic plasticity of normal cells [38]. Wang R et al. (2025) reported that POLRMT increased OXPHOS levels and mitochondrial ATP production through transcriptional upregulation of respiratory chain complexes, which counteracted lenvatinib-induced cellular ATP decrease and the AMPK-caspase 3 signaling pathway. IMT1B can resensitize the resistant HCC to lenvatinib in vitro and in vivo [39]. Arabanian et al. (2024) demonstrated that IMT1B dose-dependently inhibits proliferation of AML cell lines and primary patient samples, and synergizes with venetoclax to overcome drug resistance [40]. Our results showed that IMT1B treatment significantly inhibited AML cell proliferation and energy metabolism in vitro. More importantly, in a disseminated AML xenograft model, IMT1B not only effectively suppressed tumor growth but also ameliorated AML-induced hematopoietic abnormalities, reduced leukemic blast infiltration, and promoted the recovery of normal hematopoiesis. Our study provides strong preclinical support for the clinical development of IMT1B as a novel therapeutic agent for AML.

Conclusions

Our study identifies a novel mitochondria-localized lncRNA BCYRN1 that promotes AML progression by epigenetically upregulating MT-ND1/4/5 expression and enhancing mitochondrial OXPHOS. These findings not only advance our understanding of the metabolic reprogramming in AML but also provide a rational basis for targeting mitochondrial complex I as a therapeutic strategy.

Abbreviations

2-DG 2-deoxy-D-glucose

AML Acute myeloid leukemia

BCA Bicinchoninic Acid

BCYRN1 Brain cytoplasmic RNA 1

BLI Bioluminescence imaging

BMMCs Bone marrow mononuclear cells

BSP Bisulfite sequencing PCR

CCK-8 Cell counting kit-8

cDNA Complementary DNA

CHIRP Chromatin isolation by RNA purification

ECAR Extracellular acidification rate

ECL Enhanced chemiluminescence

FAB French-American-British

FBS Fetal bovine serum

FCCP Carbonyl cyanide 4-(trifluoromethoxy) phenylhydrazone

FISH Fluorescence in situ hybridization

GTEx Genotype-Tissue Expression

HRP Horseradish peroxidase

HSP1/2 Mitochondrial heavy-strand promoter 1/2

LSCs Leukemia stem cells

MRD Minimal residual disease

MT-ND1/4/5 Mitochondrially encoded NADH dehydrogenase 1/4/5

mtRNA Mitochondrial RNA

NCCN National Comprehensive Cancer Network

OCR Oxygen consumption rate

OS Overall survival

OXPHOS Oxidative phosphorylation

PMSF Phenylmethanesulfonyl fluoride

POLRMT RNA polymerase mitochondrial

PVDF Polyvinylidene fluoride

RT-qPCR Reverse Transcription Quantitative PCR

SDS-PAGE Sodium dodecyl sulfate-polyacrylamide gel electrophoresis

smFISH Single-molecule RNA fluorescence in situ hybridization

TBST Tris-buffered saline containing 0.1% Tween-20

TCGA The Cancer Genome Atlas

TEM Transmission electron microscopy

Declarations

Acknowledgements

We thank all the patients who participated in this study and TCGA project for providing data. We alos thank the colleagues and laboratory staff for their valuable support.

Author contributions

YK designed the research scheme, conducted the core experiments, performed data analysis and visualization, and wrote the original draft of the manuscript. JW, JL, CP and YJ participated in experimental implementation and data collection. JT and SC assisted in experimental validation and result verification. As corresponding authors, LF and SN put forward the research concept, obtained funding support, managed the project, provided overall supervision for the study, and critically revised and finalized the manuscript. All authors have read and agreed to the published version of the manuscript.

Funding

The research was supported by the National Natural Science Foundation of China (82360030); Central Guidance for Local Science and Technology Development Fund Project (202407AD110004); Kunming Medical Technology Center (2024-SW-19); High-level Talent Cultivation and Attraction Support Plan for Yunnan Province (YNQR-QNRC-2020-091); High level Health Technology Talents in Yunnan Province - Medical Discipline Leaders (D-2024009).

Data availability

The transcriptomic data are deposited in the TCGA database and will be publicly available upon manuscript publication. All other study data are available from the corresponding author upon reasonable request prior to public release.

Ethics approval and consent to participate

The study was approved by the Human Ethics Committee of the Yan'an Hospital Affiliated to Kunming Medical University (Approval No. 2024-013-01), and informed written consent was obtained from all

participants. The study was conducted in accordance with the Declaration of Helsinki and the Ethical Guidelines for Medical Research on Human Subjects. All animal experiments were approved by the Animal Ethics Committee of the Yan'an Hospital Affiliated to Kunming Medical University (Approval No. 2023021) and were carried out in accordance with the Guide for the Care and Use of Laboratory Animals and the ARRIVE guidelines.

Consent for publication

All authors consent to the publication of the manuscript.

Competing interests

The authors declare no competing financial or personal interests that could have influenced the work.

Author details

[1]Yan'an Hospital Affiliated to Kunming Medical University, No. 245 East Renmin Road, Kunming, 650051, China.

References

1. Wachter F, Pikman Y. Pathophysiology of Acute Myeloid Leukemia. Acta Haematol. 2024;147(2):229–46.
2. Stubbins RJ, Francis A, Kuchenbauer F, et al. Management of Acute Myeloid Leukemia: A Review for General Practitioners in Oncology. Curr Oncol. 2022;29(9):6245–59.
3. Shallis RM, Wang R, Davidoff A, et al. Epidemiology of acute myeloid leukemia: Recent progress and enduring challenges. Blood Rev. 2019;36:70–87.
4. Kantarjian HM, DiNardo CD, Kadia TM, et al. Acute myeloid leukemia management and research in 2025. CA Cancer J Clin. 2025;75(1):46–67.
5. Urlu SM, Özcan M. Acute myeloid leukemia: a brief historical perspective of AML treatment. Hematology. 2025;30(1):2539528.
6. Cui C, Wang Y, Gong W, et al. Long Non-Coding RNA LINC00152 Regulates Self-Renewal of Leukemia Stem Cells and Induces Chemo-Resistance in Acute Myeloid Leukemia. Front Oncol. 2021;11:694021.
7. Percival MM, Estey EH. Current treatment strategies for measurable residual disease in patients with acute myeloid leukemia. Cancer. 2019;125(18):3121–30.
8. Stubbins RJ, Maksakova IA, Sanford DS, et al. Mitochondrial metabolism: powering new directions in acute myeloid leukemia. Leuk Lymphoma. 2021;62(10):2331–41.
9. Nelson MA, McLaughlin KL, Hagen JT, et al. Intrinsic OXPHOS limitations underlie cellular bioenergetics in leukemia. Elife. 2021;10:e63104.

10. Yamaguchi H. Advances in pathogenesis research and challenges in treatment development for acute myeloid leukemia. Int J Hematol. 2024;120(4):414–6.
11. Sharma P, Borthakur G. Targeting metabolic vulnerabilities to overcome resistance to therapy in acute myeloid leukemia. Cancer Drug Resist. 2023;6(3):567–89.
12. Kaur K, Martinez CV, Do KNK, et al. Relationship between Mitochondrial Oxphos Kinetics and Response to Induction Chemotherapy in Patients with. Acute Myeloid Leuk Blood. 2023;142(Sup1):2.
13. Wang JD, Xu JQ, Long ZJ, et al. Disruption of mitochondrial oxidative phosphorylation by chidamide eradicates leukemic cells in AML. Clin Transl Oncol. 2023;25(6):1805–20.
14. Peng M, Huang Y, Zhang L, et al. Targeting Mitochondrial Oxidative Phosphorylation Eradicates Acute Myeloid Leukemic Stem Cells. Front Oncol. 2022;12:899502.
15. Luna-Yolba R, Marmoiton J, Gigo V, et al. Disrupting Mitochondrial Electron Transfer Chain Complex I Decreases Immune Checkpoints in Murine and Human Acute Myeloid Leukemic Cells. Cancers (Basel). 2021;13(14):3499.
16. Han XY, Li X, Zhao RY, et al. Comprehensive analysis of prognostic value and immunotherapy prospect of brain cytoplasmic RNA1 in hepatocellular carcinoma. World J Gastrointest Oncol. 2023;15(4):644–64.
17. Wang Y, Bai W, Wang M, et al. Long Non-Coding RNA Brain Cytoplasmic RNA 1 Acts as an Oncogene and Regulates Cell Proliferation and Metastasis in Non-Small Cell Lung Cancer. J Nanosci Nanotechnol. 2019;19(4):1978–85.
18. Huo W, Qi F, Wang K. Long non-coding RNA BCYRN1 promotes prostate cancer progression via elevation of HDAC11. Oncol Rep. 2020;44(3):1233–45.
19. Fernandez C, Santos-Silva MC, López A, et al. Newly diagnosed adult AML and MPAL patients frequently show clonal residual hematopoiesis. Leukemia. 2013;27(11):2149–56.
20. Elias S, Brown S, Egini O, et al. Allogeneic hematopoietic cell transplantation in acute myeloid leukemia not in complete remission: outcomes and prognostic factors in a contemporary cohort. Blood Cancer J. 2025;15(1):208.
21. Yang H, Tabe Y, Saito K et al. Mitochondrial Transfer Confers Microenvironment-Mediated Resistance to Oxphos Inhibition in AML.Blood, 2018, 132(Suppl_1):430–430.
22. Lagadinou ED, Sach A, Callahan K, et al. BCL-2 inhibition targets oxidative phosphorylation and selectively eradicates quiescent human leukemia stem cells. Cell Stem Cell. 2013;12(3):329–41.
23. Tabe Y, Konopleva M. Resistance to energy metabolism - targeted therapy of AML cells residual in the bone marrow microenvironment. Cancer Drug Resist. 2023;6(1):138–50.
24. Chrest BR, Fisher-Wellman KH. Re-evaluating the rationale for targeting oxidative phosphorylation in acute myeloid leukemia. Biochem J. 2026;483(6):907–25.
25. Baccelli I, Gareau Y, Lehnertz B, et al. Mubritinib Targets the Electron Transport Chain Complex I and Reveals the Landscape of OXPHOS Dependency in Acute Myeloid Leukemia. Cancer Cell.

2019;36(1):84–99.
26. Sheth AI, Althoff MJ, Tolison H, et al. Targeting Acute Myeloid Leukemia Stem Cells through Perturbation of Mitochondrial Calcium. Cancer Discov. 2024;14(10):1922–39.
27. Balasundaram N, Palani HK, Venkatraman A, et al. A novel strategy to target metabolic dependencies in acute myeloid leukemia. Cell Death Dis. 2025;6(1):792.
28. Wu S, Akhtari M, Alachkar H. Characterization of Mutations in the Mitochondrial Encoded Electron Transport Chain Complexes in Acute Myeloid Leukemia. Sci Rep. 2018;8(1):13301.
29. Guo W, Liu Y, Ji X, et al. Mutational signature of mtDNA confers mechanistic insight into oxidative metabolism remodeling in colorectal cancer. Theranostics. 2023;13(1):324–38.
30. Arance E, Ramírez V, Rubio-Roldan A, et al. Determination of Exosome Mitochondrial DNA as a Biomarker of Renal Cancer Aggressiveness. Cancers (Basel). 2021;14(1):199.
31. Yang Q, Zhao T, Han Y, et al. Dynamics of mitochondrial DNA copy number regulation in relation to gastric cancer survival. Discov Oncol. 2025;16(1):1090.
32. Liao K, Yu J, Akhmerov A, et al. Long noncoding RNA BCYRN1 promotes cardioprotection by enhancing human and murine regulatory T cell dynamics. J Clin Invest. 2025;135(9):e179262.
33. Hu T, Lu YR. BCYRN1, a c-MYC-activated long non-coding RNA, regulates cell metastasis of non-small-cell lung cancer. Cancer Cell Int. 2015;15:36.
34. Sandhanam K, Tamilanban T. Unraveling the noncoding RNA landscape in glioblastoma: from pathogenesis to precision therapeutics. Naunyn Schmiedebergs Arch Pharmacol. 2024;397(12):9475–502.
35. Daglish SCD, Fennell EMJ, Graves LM. Targeting Mitochondrial DNA Transcription by POLRMT Inhibition or Depletion as a Potential Strategy for Cancer Treatment. Biomedicines. 2023;11(6):1598.
36. Han L, Cavazos A, Baran N, et al. Mitochondrial Oxphos As Survival Mechanism of Minimal Residual AML Cells after Induction Chemotherapy: Survival Benefit By Complex I Inhibition with Iacs-010759. Blood. 2019;134(Supple1):5161–5161.
37. Yap TA, Daver N, Mahendra M, et al. Complex I inhibitor of oxidative phosphorylation in advanced solid tumors and acute myeloid leukemia: phase I trials. Nat Med. 2023;29(1):115–26.
38. Li X, Ze X, Zhou S, et al. Discovery of a Novel, Potent, Orally Active, and Safe Inhibitor Targeting Human Mitochondrial RNA Polymerase. J Med Chem. 2023;66(7):5118–53.
39. Wang R, Chen B, Pan Y, et al. POLRMT enhances lenvatinib resistance in hepatocellular carcinoma cells by maintaining mitochondrial ATP production. Life Sci. 2025;379:123876.
40. Laleh S, Arabanian J, Adamsson A, Unger, et al. Reduced mitochondrial transcription sensitizes acute myeloid leukemia cells to BCL-2 inhibition. eLife. 2024;13:RP97749.

Tables

Tables 1 to 3 are available in the supplementary files section

Figures

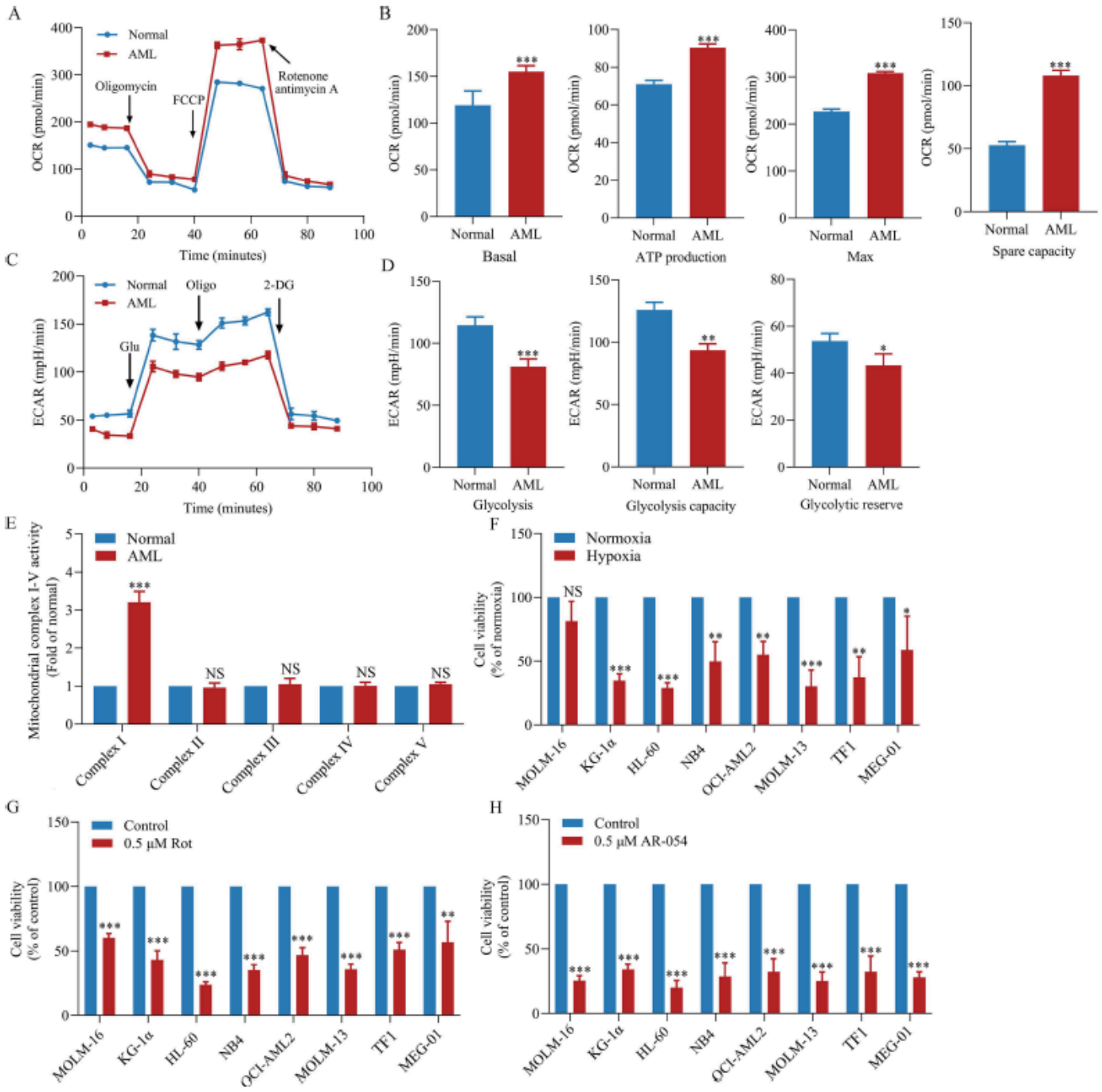


Figure 1

AML cells show enhanced dependency on mitochondrial OXPHOS rather than glycolysis

A.Oxygen consumption rate (OCR) curves of normal and AML bone marrow mononuclear cells (BMMCs) measured by Seahorse XF analysis. **B.** Quantitative analysis of basal OCR, ATP production-linked OCR, maximal OCR and spare respiratory capacity. **C.** Extracellular acidification rate (ECAR) curves of normal and AML BMMCs. **D.** Quantitative analysis of basal glycolysis level, glycolysis capacity, and glycolytic

reserve derived from ECAR curves. **E.**Enzymatic activities of mitochondrial respiratory chain complexes I–V detected by colorimetric assays. **F.** Cell viability of various AML cell lines cultured under normoxia or hypoxia conditions for 48 h. **G-H.** Cell viability of various AML cell lines treated with 0.5 μM rotenone or 0.5 μM AR-054 for 48 h. ***P<0.001, **P<0.01, *P<0.05, NS: not significant. Panels A-E: AML groups vs. Normal groups; panel F: hypoxic groups vs. normoxic groups; panels G-H: drug-treated groups vs. control groups.

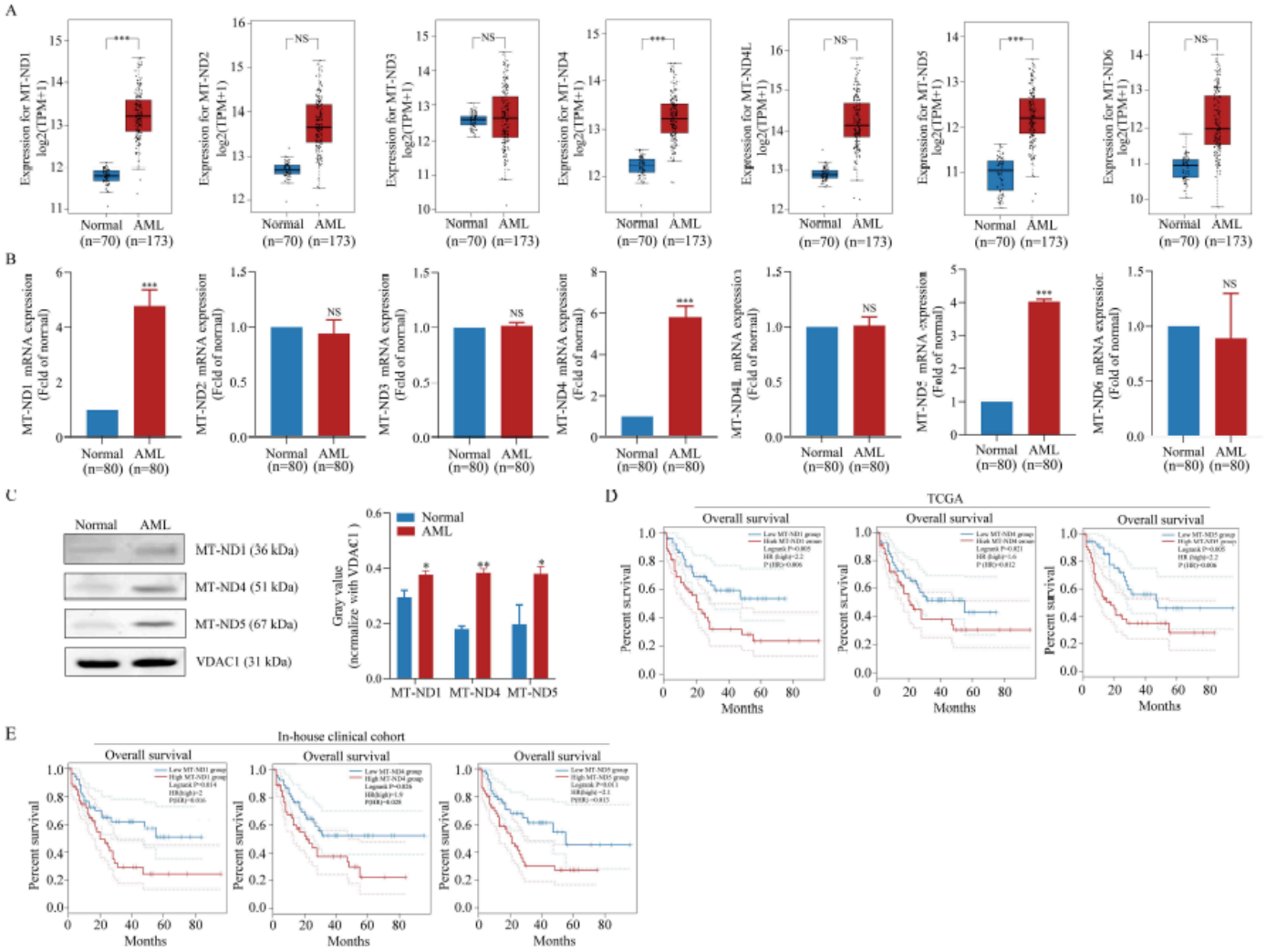


Figure 2

MT-ND1, MT-ND4 and MT-ND5 are specifically upregulated in AML and associated with poor prognosis

A.Transcriptomic expression levels of seven mitochondrial complex I subunits (MT-ND1 to MT-ND6, including MT-ND4L) in normal peripheral whole blood (n=70) and BMMCs of AML patients (n=173) from the TCGA+GTEx cohort. **B.** RT-qPCR validation of mRNA expression of the above subunits in BMMC samples from 80 normal controls and AML patients. **C.** Western blot analysis of MT-ND1, MT-ND4 and MT-ND5 protein levels in normal controls and AML patients, with VDAC1 as the loading control. Right

panel: quantitative gray value analysis normalized to VDAC1. **D-E.** Kaplan-Meier overall survival analysis of AML patients stratified into high and low expression groups based on the median expression value of MT-ND1, MT-ND4 or MT-ND5 in the TCGA cohort (D) or our in-house cohort (E). Hazard ratio (HR) and log-rank test P values are indicated in each panel. ***P< 0.001, **P< 0.01, *P< 0.05, NS, not significant. AML groups vs. Normal groups.

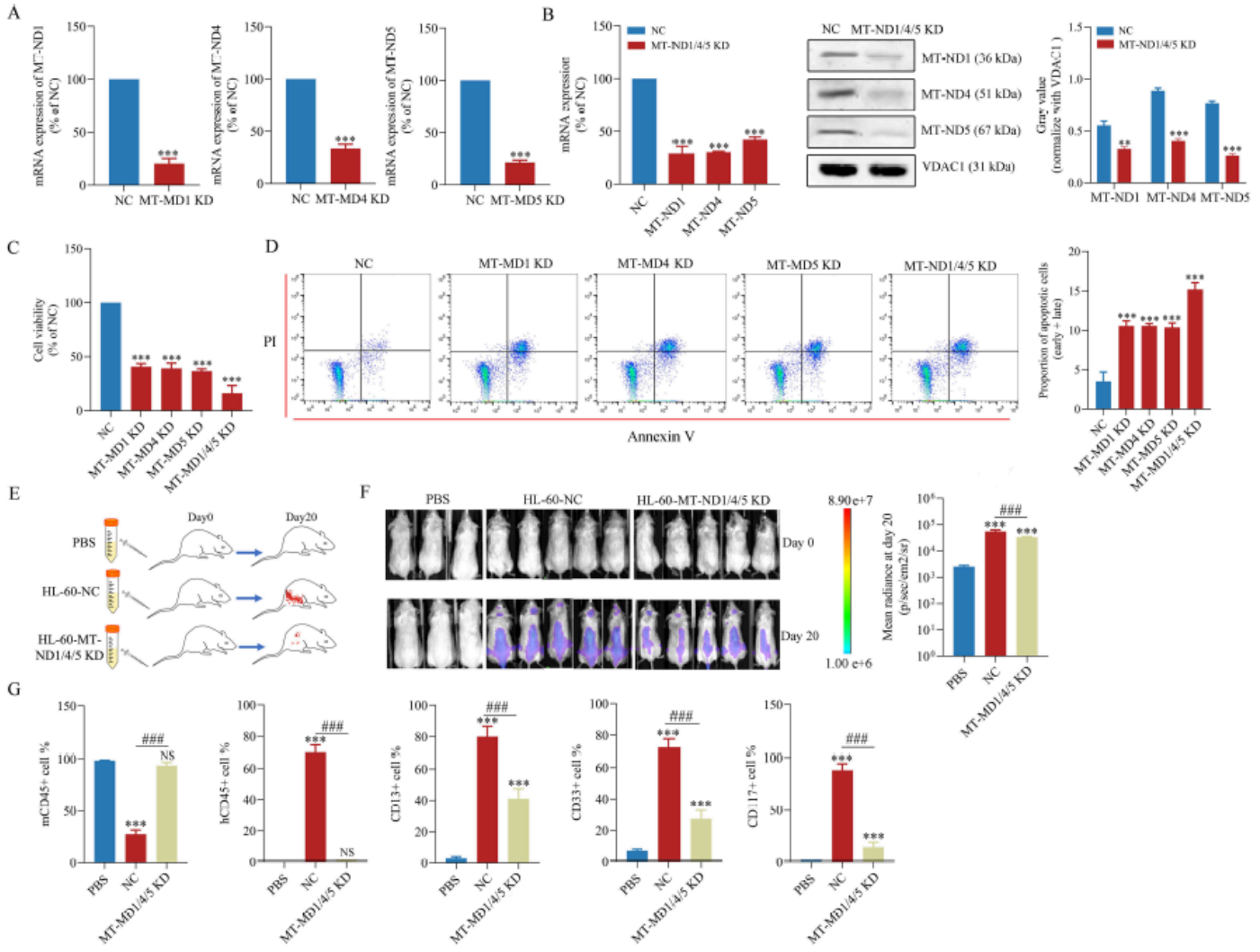


Figure 3

Triple knockdown of MT-ND1/4/5 reduces viability and promotes apoptosis in HL-60 cells and xenografts

A. RT-qPCR analysis of MT-ND1/4/5 mRNA levels in MT-ND1/4/5 KD and negative control HL-60 cells. **B.** Validation of triple knockdown efficiency of MT-ND1/4/5 by RT-qPCR (left) and Western blot (right). **C.** Cell viability of HL-60 cells with single or triple knockdown of MT-ND1/4/5 detected by CCK-8 assay. **D.** Apoptosis rates of HL-60 cells with single or triple knockdown of MT-ND1/4/5 measured using Annexin V-PI by flow cytometry. **E.** Schematic diagram of the disseminated AML xenograft model. **F.** In vivo bioluminescence imaging of mice at day 0 and day 20 (left) and quantitative analysis of mean radiance

(right). **G.** Flow cytometric analysis of mCD45+, hCD45+, hCD13+, hCD33+ and hCD117+ cell proportions in the bone marrow of mice from each group. **P<0.01, ***P<0.001, NS, not significant. Panels A–D: Knockdown groups vs. NC group, Panels F–G: MT-ND1/4/5 KD groups or NC group vs. PBS group; ###P<0.001, MT-ND1/4/5 KD groups vs. NC group.

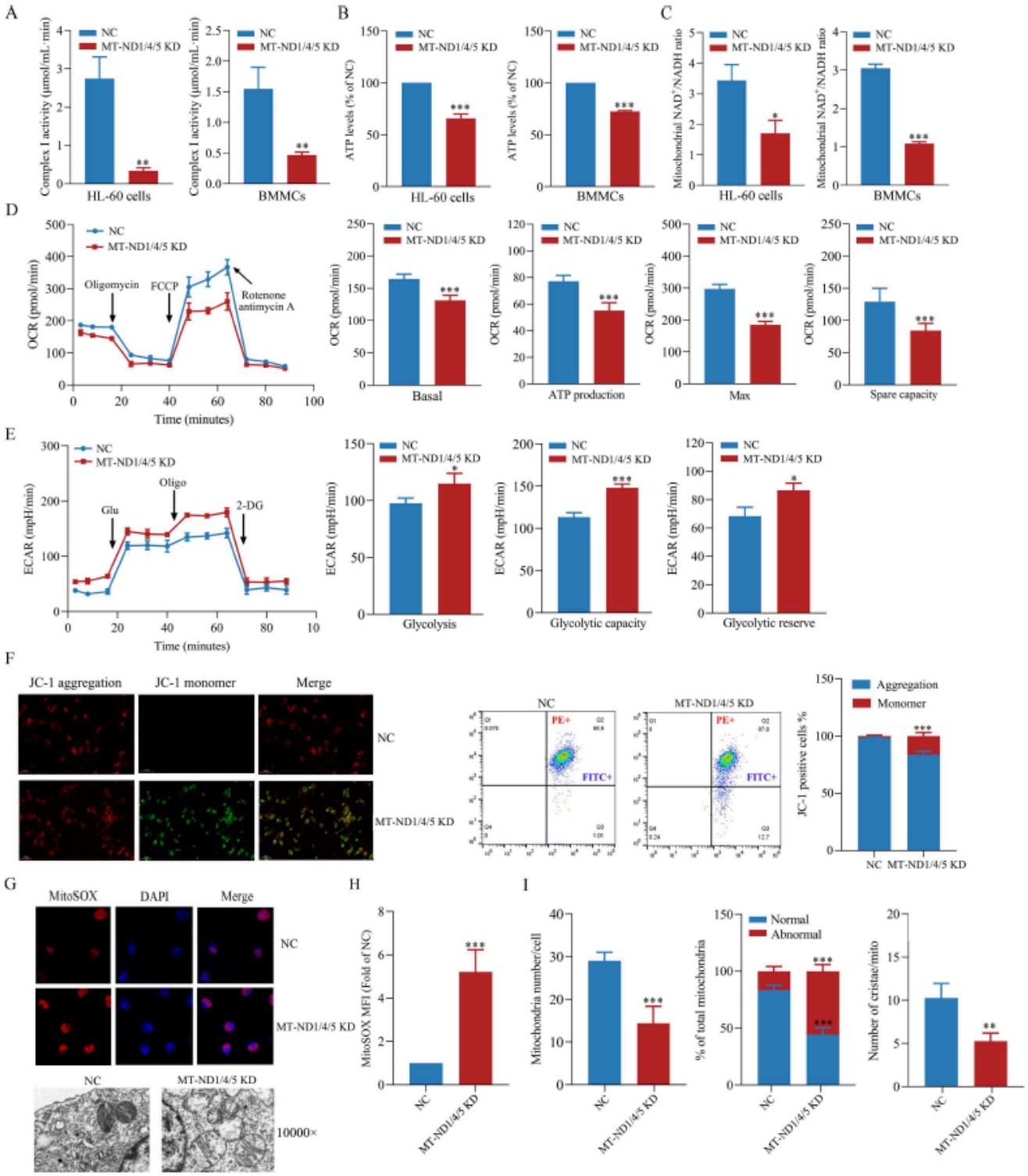


Figure 4

Knockdown of MT-ND1/4/5 impairs OXPHOS and causes mitochondrial dysfunction and structural damage in AML cells

All in vitro assays were performed in nagtive control (NC) and MT-ND1/4/5 triple-knockdown HL-60 cells (MT-ND1/4/5 KD), and ex vivo validation was conducted using BMMCs from the corresponding disseminated AML xenograft model.

A. Enzymatic activity of mitochondrial complex I in HL-60 cells and xenograft-derived BMMCs, measured by colorimetric assay. **B-C.** Intracellular ATP production and mitochondrial NAD^+/NADH ratio in HL-60 cells and xenograft-derived BMMCs. **D.** OCR curves (left) and quantitative analysis of basal OCR, ATP production-linked OCR, maximal OCR and spare capacity (right) measured by Seahorse XF analyzer. **E.** ECAR curves (left) and quantitative analysis of glycolysis, glycolytic capacity, and glycolytic reserve (right). **F.** Mitochondrial membrane potential detected by JC-1 staining. Representative fluorescence images (left, 200× magnification) and flow cytometric quantification of the proportions of JC-1 aggregates and monomers are presented. **G.** Detection of mitochondrial superoxide and mitochondrial ultrastructure. Upper: representative fluorescence images of MitoSOX Red staining (red) with DAPI nuclear counterstaining (blue). Lower: representative TEM images of mitochondrial ultrastructure (×10000 magnification). **H.** Quantitative analysis of MitoSOX Red mean fluorescence intensity (MFI) by flow cytometry. **I.** Quantitative analysis of mitochondrial number per cell, the percentage of normal/abnormal mitochondria (with swollen morphology and disrupted cristae) and the number of cristae per mitochondrion based on TEM images. ***P<0.001, *P<0.01, P < 0.05. MT-ND1/4/5 KD group vs. NC group.

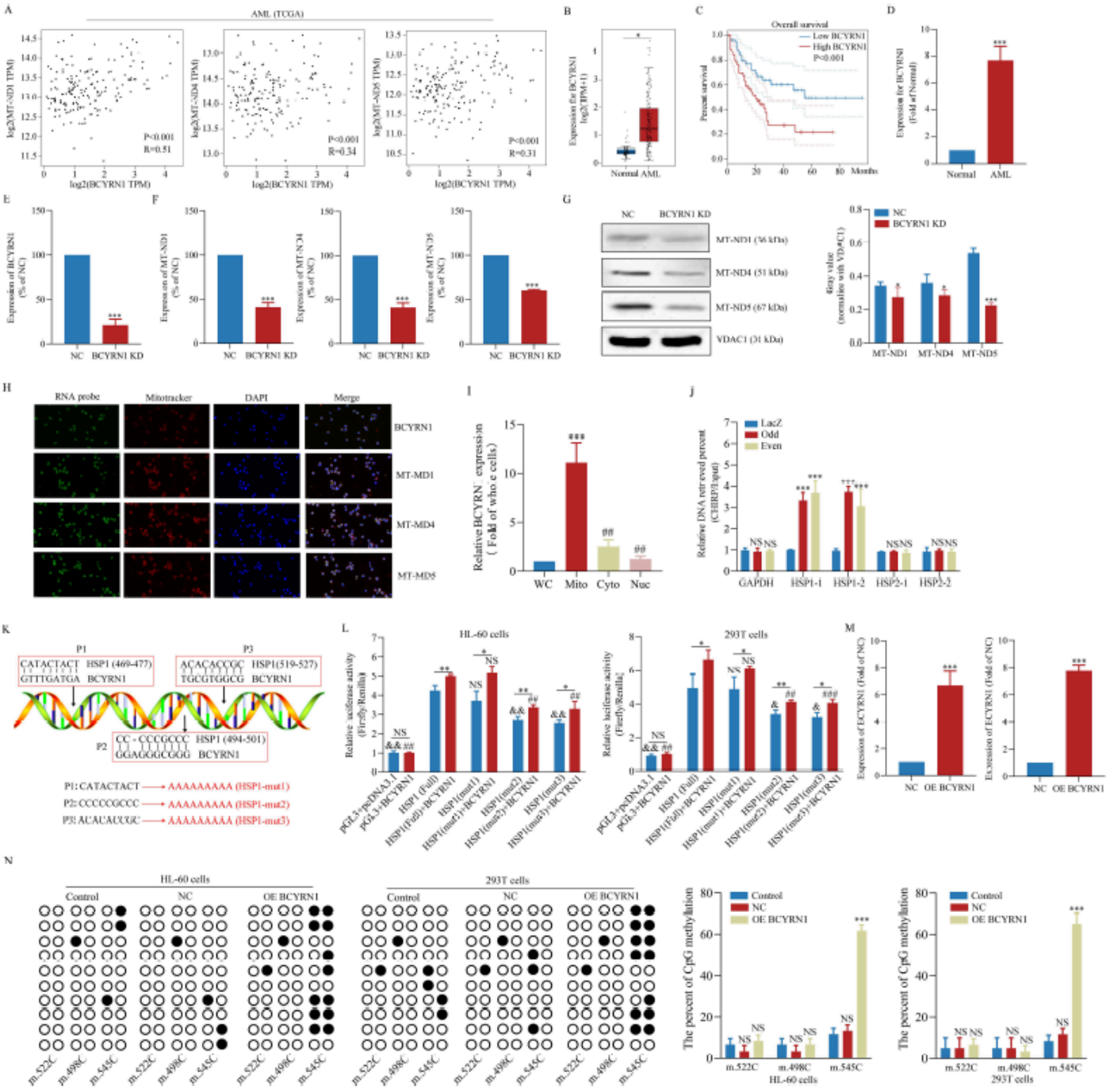


Figure 5

LncRNA BCYRN1 is upregulated in AML and transcriptionally activates MT-ND1/4/5 via direct promoter binding and epigenetic regulation

A. Correlation analysis between BCYRN1 expression and MT-ND1, MT-ND4, MT-ND5 expression in the TCGA AML cohort. **B.** BCYRN1 expression levels in normal samples (n=70) and AML samples (n=173) from the TCGA+GTEx cohort. **C.** Kaplan-Meier overall survival analysis of AML patients stratified by median BCYRN1 expression in the TCGA cohort. **D.** RT-qPCR validation of BCYRN1 expression in our in-

house clinical cohort (80 normal controls and 80 AML patients). **E-F.** RT-qPCR analysis of BCYRN1, MT-ND1, MT-ND4 and MT-ND5 mRNA expression in negative control (NC) or knockdown BCYRN1 (BCYRN1 KD) HL-60 cells. **G.** Western blot analysis of MT-ND1, MT-ND4 and MT-ND5 protein expression in NC and BCYRN1 KD HL-60 cells. VDAC1 was used as the loading control. **H.** RNA fluorescence in situ hybridization (FISH) combined with MitoTracker staining (red) showing the subcellular localization of BCYRN1, MT-ND1, MT-ND4 and MT-ND5 (green) in HL-60 cells. Nuclei were counterstained with DAPI (blue). **I.** Subcellular fractionation assay detecting BCYRN1 expression in whole cell (WC), mitochondrial (Mito), cytoplasmic (Cyto) and nuclear (Nuc) fractions. **J.** Mitochondrial RNA pull-down assay showing enrichment of BCYRN1 at mitochondrial HSP1 regions, with GAPDH as the negative control. **K.** Schematic diagram showing the predicted binding sites of BCYRN1 in the HSP1 region and the design of mutant (mut) reporter constructs. **L.** Dual-luciferase reporter assay in HL-60 and 293T cells verifying the regulatory effect of BCYRN1 on wild-type and mutant HSP1 activities. **M.** RT-qPCR was performed to verify BCYRN1 expression levels in negative control and BCYRN1 overexpressing (OE BCYRN1) HL-60 and HEK293T cells. **N.** Bisulfite sequencing PCR (BSP) analysis of CpG methylation levels in the HSP1 regions in NC and BCYRN1 overexpressing HL-60 and 293T cells. Each circle represents a CpG site; filled circles indicate methylated sites, open circles indicate unmethylated sites. ***P<0.001, **P<0.01, *P<0.05; NS, not significant. Panel E: AML group vs. normal group, panels F–H: BCYRN1 KD group vs. NC group, panel J: Mit, Ctyo or Nuc groups vs. WC group, panel K: odd or even groups vs. LacZ group, panel N: NC or OE BCYRN1 groups vs. Control groups; $^{\#\#}$P<0.01. NS. panels J: Ctyo or Nuc groups vs. mito group, panels M: BCYRN1+pGLS3/HSP1 mut vs. BCYRN1+HSP1 full; $^{\&\&}$P<0.01, $^{\&}$P<0.05, NS. panels M: pGLS3+pcDNA3.1 or HSP1 mut vs. HSP1 full.

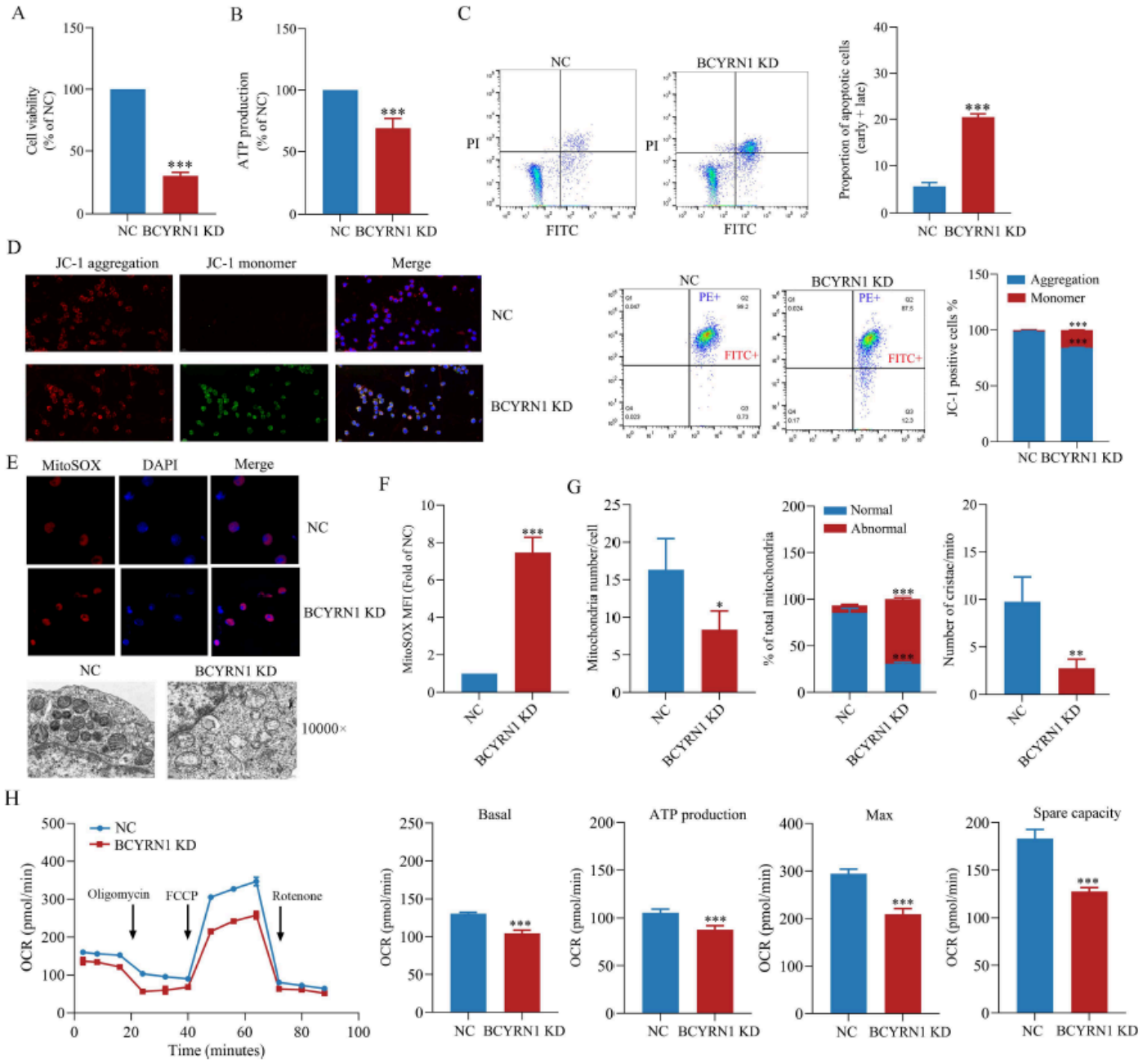


Figure 6

Knockdown of lncRNA BCYRN1 inhibits proliferation, induces apoptosis and impairs mitochondrial function in AML cells

All experiments were performed in negative control (NC) and knockdown of BCYRN1 (BCYRN1 KD) HL-60 cells. **A.** Cell viability detected by CCK-8 assay. **B.**Intracellular ATP production levels measured by chemiluminescence assay. **C.**Apoptosis rates measured by Annexin V/PI flow cytometry. Representative dot plots (left) and quantitative analysis of total apoptotic cells (early + late apoptosis, right) are shown. **D.** Mitochondrial membrane potential detected by JC-1 staining. Representative fluorescence images

(left), flow cytometric dot plots (middle) and quantitative analysis of the percentage of JC-1 monomer-positive cells and JC-1 aggregate-positive cells are presented on the right. **E.** Mitochondrial superoxide levels and ultrastructure analysis. (Upper) Representative fluorescence images of MitoSOX Red staining (red) with DAPI nuclear counterstaining (blue). (Lower) TEM images of mitochondrial ultrastructure at 10000× magnification. **F.** Quantitative analysis of MitoSOX Red MFI by flow cytometry. **G.** Quantitative analysis of mitochondrial number per cell, percentage of normal/abnormal mitochondria and number of cristae per mitochondrion based on TEM images. **H.** OCR curves (left) and quantitative analysis of basal OCR, ATP production-linked OCR, maximal OCR and spare capacity (right) measured by Seahorse XF analyzer. ***P<0.001, **P<0.01, *P<0.05 for BCYRN1 KD group vs. NC group.

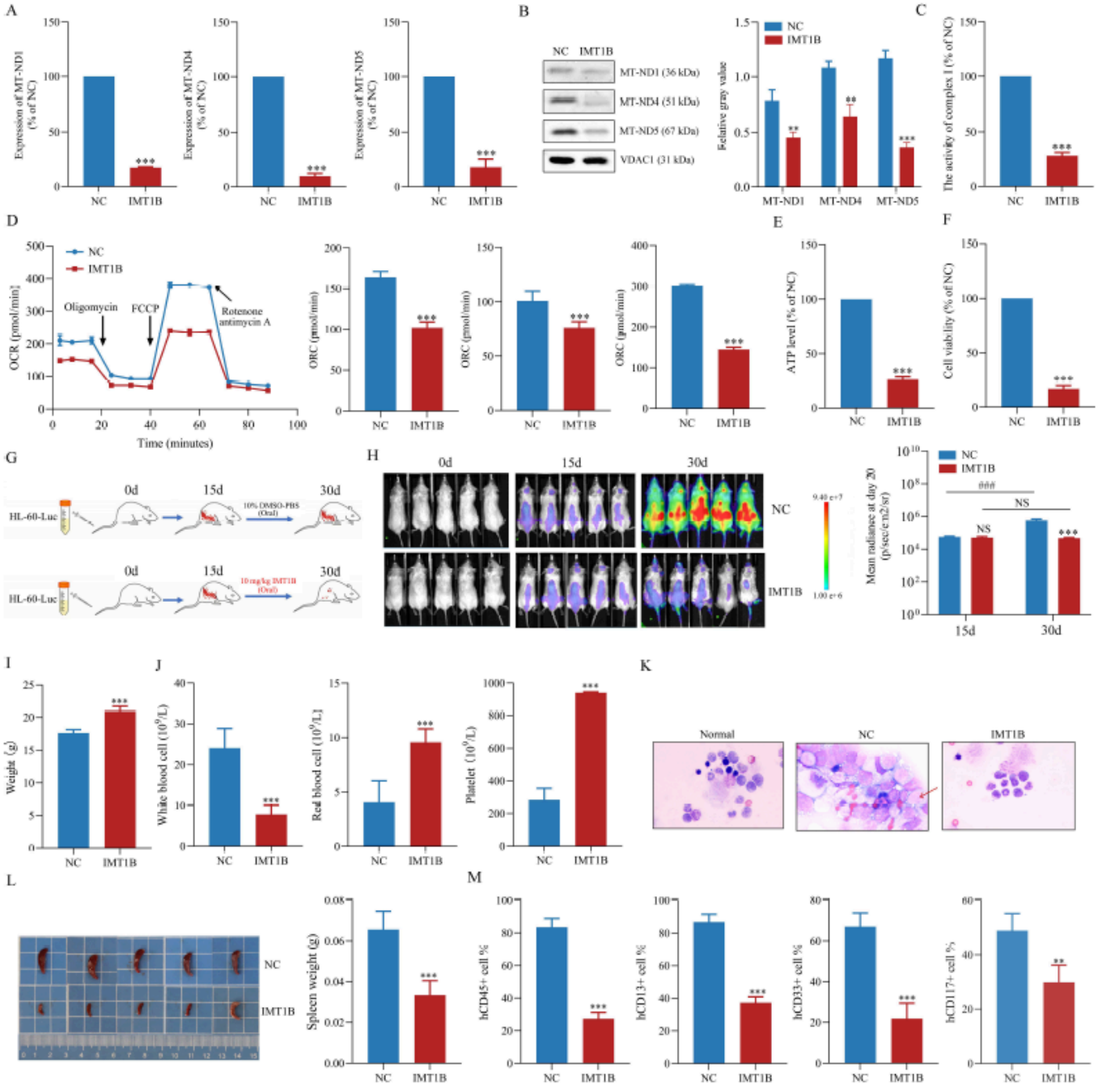


Figure 7

POLRMT inhibitor IMT1B downregulates MT-ND1/4/5 and exerts potent anti-leukemic effects in vitro and in vivo

All in vitro experiments were performed in HL-60 cells treated with PBS (NC) or 1 μM IMT1B for 48 hours. The in vivo disseminated AML xenograft model was established by tail vein injection of HL-60-luc cells, and mice were randomly divided into NC group (PBS) and IMT1B treatment group (10 mg/kg IMT1B oral administration daily starting from day 15). **A.** RT-qPCR analysis of MT-ND1, MT-ND4 and MT-ND5 mRNA expression levels. **B.** Western blot analysis of MT-ND1, MT-ND4 and MT-ND5 protein expression (left) and quantitative analysis of relative gray values (right), with VDAC1 as the loading control. **C.** Enzymatic activity detection of mitochondrial respiratory chain complex I protein levels. **D.** OCR curves measured by Seahorse XF analyzer (left). Quantitative analysis of basal OCR, ATP production-linked OCR and maximal OCR (right). **E.** Intracellular ATP production levels by chemiluminescence assay. **F.** Cell viability detected by CCK-8 assay. **G.** Schematic diagram of the in vivo experimental design. **H.** In vivo bioluminescence imaging of mice at day 0, 15 and 30 (left) and quantitative analysis of mean radiance at day 15 and day 30 (right). **I.** Body weight of mice in each group at the end of the experiment. **J.** Peripheral blood cell counts including WBC, RBC and PLT. **K.** Wright-Giemsa staining of bone marrow smears. Red arrows indicate atypical myelocytes. **L.** Representative images of spleens (left) and quantitative analysis of spleen weight (right). M. Flow cytometric analysis of hCD45+, hCD13+, hCD33+ and hCD117+ cell proportions in the bone marrow of mice. ***P <0.001, **P<0.01, *P<0.05, NS, not significant. IMT1B group vs. NC group; panel H: $^{###}$P <0.001, NC group at day 30 vs. day 15.

Supplementary Files

This is a list of supplementary files associated with this preprint. Click to download.

- TableS1.docx
- TableS2.docx
- TableS3.docx